

# Magneto-transport in a quantum network: Evidence of a mesoscopic switch

Srilekha Saha,<sup>1</sup> Santanu K. Maiti,<sup>2,\*</sup> and S. N. Karmakar<sup>1</sup>

<sup>1</sup>Theoretical Condensed Matter Physics Division, Saha Institute of Nuclear Physics,  
Sector-I, Block-AF, Bidhannagar, Kolkata-700 064, India

<sup>2</sup>School of Chemistry, Tel Aviv University, Ramat-Aviv, Tel Aviv-69978, Israel

We investigate magneto-transport properties of a  $\theta$  shaped three-arm mesoscopic ring where the upper and lower sub-rings are threaded by Aharonov-Bohm fluxes  $\phi_1$  and  $\phi_2$ , respectively, within a non-interacting electron picture. A discrete lattice model is used to describe the quantum network in which two outer arms are subjected to binary alloy lattices while the middle arm contains identical atomic sites. It is observed that the presence of the middle arm provides localized states within the band of extended regions and lead to the possibility of switching action from a high conducting state to a low conducting one and vice versa. This behavior is justified by studying persistent current in the network. Both the total current and individual currents in three separate branches are computed by using second-quantized formalism and our idea can be utilized to study magnetic response in any complicated quantum network. The nature of localized eigenstates are also investigated from probability amplitudes at different sites of the quantum device.

PACS numbers: 73.23.-b, 73.23.Ra.

## I. INTRODUCTION

Theoretical and experimental investigations in low-dimensional systems lead to the opportunity of visualizing various novel quantum mechanical effects<sup>1,2</sup> in a tunable way. Persistent current being one such exotic quantum mechanical phenomenon observed in normal metal mesoscopic rings and nanotubes pierced by Aharonov-Bohm (AB) flux  $\phi$ . Prior to its experimental evidence,

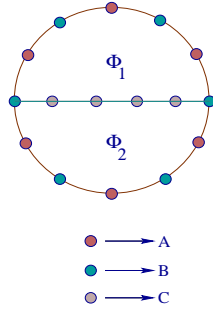


FIG. 1: (Color online). Schematic view of a quantum network where the upper and lower sub-rings are threaded by AB fluxes  $\phi_1$  and  $\phi_2$ , respectively. Both the upper and lower arms are subjected to binary alloy lattices, while the middle arm contains identical lattice sites. The filled colored circles correspond to the positions of the atomic sites.

the possibility of a non-decaying current in normal metal rings was first predicted by Büttiker, Imry and Landauer<sup>3</sup> in a pioneering work, and, in the sub-sequent years theoretical attempts were made<sup>4-17</sup> to understand the actual mechanism behind it. The experimental realization of this phenomenon of non-decaying current in metallic rings/cylinders has been established quite in late. It has been first examined by Levy *et al.*<sup>18</sup> and later many other experiments<sup>19-21</sup> have confirmed the existence of non-dissipative currents in such quantum systems.

Although the studies involving simple mesoscopic rings have already generated a wealth of literature there is still need to look deeper into the problem to address several important issues those have not yet been explored, as for example the understanding of the behavior of persistent current in multiply connected quantum network, specially in presence of disorder. It is well known that in presence of random site-diagonal disorder in an one-dimensional (1D) mesoscopic ring all the energy levels are localized<sup>22</sup>, and accordingly, the persistent current gets reduced enormously in presence of disorder compared to that of an ordered ring. But there are some 1D disordered systems which support extended eigenstates along with the localized energy levels, and these materials may provide several interesting issues, mainly to provide a localization to delocalization transition and vice versa. For example, in a pioneering work Dunlap *et al.*<sup>23</sup> have shown that even in 1D disordered systems extended eigenstates are possible for certain kind of topological correlations among the atoms. They have proposed that any physical system which can be described by the random dimer model should exhibit the transmission resonances and a huge enhancement in the transmission takes place when the Fermi level coincides with the unscattered states. In a consecutive year Wu *et al.*<sup>24</sup> have argued that the random dimer model can also be used to explain the insulator to metal transition in polyaniline as a result of the movement of the Fermi level to extended region. Later, several other works<sup>25-29</sup> have also been carried out in such type of materials to exhibit many important physical results.

The existence of localized energy eigenstates together with the extended states in a simple ring geometry has been explored in some recent works by Jiang *et al.*<sup>26,27</sup>. They have analyzed the nature of these states by evaluating persistent current and the wave amplitudes at different sites of the ring. In these systems localized states appear by virtue of disorder. But, in our present work we make an attempt to establish localized eigenstates, even

in the absence of disorder, along with extended states simply by considering the effect of topology of the system. To the best of our knowledge, this behavior has not been addressed earlier in the literature. Here we consider a three-arm mesoscopic ring in which two outer arms are subjected to binary alloy lattices and the middle one contains identical lattice sites, and, we show that due to the presence of the middle arm quasi-localized energy eigenstates are observed within the band of extend regions. It leads to the possibility of getting switching action from a high conducting state to a low one and vice versa as a result of the movement of the Fermi level. We illustrate this behavior by studying persistent current in the quantum network and explore the nature of energy eigenstates in terms of the probability amplitude in different lattice sites of the geometry. Our present analysis can be utilized to study magnetic response in any complicated quantum network and we believe that this work offers an excellent opportunity to study the simultaneous effects of topology and the magnetic fields threaded by two sub-rings in our three-arm ring system.

With an introduction in Section I we organize the paper as follows. In Section II, first we present the model, then describe the theoretical formalism which include the Hamiltonian and the formulation of persistent currents in individual branches of the network. In Section III we analyze the results and finally in Section IV we draw our conclusions.

## II. MODEL AND THEORETICAL FORMULATION

### A. The model and the Hamiltonian

Let us refer to Fig. 1. A three-arm mesoscopic ring where the upper and lower sub-rings are threaded by AB fluxes  $\phi_1$  and  $\phi_2$ , respectively. The outer arms are subjected to binary alloy lattices (consisting of A and B types of atoms) and the middle arm contains identical lattice sites (atomic sites labeled by C) except those on the boundaries. The filled colored circles correspond to the positions of the atomic sites. Within a tight-binding framework the Hamiltonian for such a network reads as,

$$H = \sum_j \epsilon_j c_j^\dagger c_j + t \sum_j \left( c_j^\dagger c_{j+1} e^{-i\theta_1} + h.c. \right) + \sum_l \epsilon_l c_l^\dagger c_l + v \sum_l \left( c_l^\dagger c_{l+1} e^{-i\theta_2} + h.c. \right) \quad (1)$$

where,  $\epsilon_j$  represents the site energy for the outer arms, while for the middle arm it is assigned by  $\epsilon_l$ . In the outer ring  $\epsilon_j = \epsilon_A$  or  $\epsilon_B$  alternately so that it forms a binary alloy. On the other hand,  $\epsilon_l = \epsilon_C$  for the atomic sites those are referred by C atoms.  $t$  and  $v$  are the nearest-neighbor hopping integrals in the outer and middle arms, respectively. Due to the presence of magnetic fluxes  $\phi_1$  and  $\phi_2$  in two sub-rings, phase factors  $\theta_1$  and  $\theta_2$  appears

into the Hamiltonian. They are expressed as follows:  $\theta_1 = 2\pi(\phi_1 + \phi_2)/(N_U + N_L)$  and  $\theta_2 = 2\pi(\phi_1 - \phi_2)/2N_M$ . Here the fluxes are measured in units of the elementary flux-quantum  $\phi_0 (= ch/e)$ , and,  $N_U$ ,  $N_M$  and  $N_L$  represent the total number of single bonds (each single bond is formed by connecting two neighboring lattice sites) in the upper, middle and lower arms, respectively. It reveals that  $N_U + N_M + N_L - 1$  number of atomic sites in the quantum network.  $c_j^\dagger$  ( $c_j$ ) corresponds to the creation (annihilation) operator of an electron at the  $j$  th site, and, a similar definition also goes for the atomic sites  $l$ .

### B. Calculation of persistent current

In the second quantized notation the general expression of charge current operator is in the form<sup>30</sup>,

$$I = \frac{2\pi i e \alpha}{L} \sum_n \left( c_n^\dagger c_{n+1} - c_{n+1}^\dagger c_n \right). \quad (2)$$

Here,  $L$  is the length of the arm in which we are interested to calculate the current and  $\alpha$  represents the nearest-neighbor hopping strength. The nearest-neighbor hopping strength ( $\alpha$ ) is equal to  $t$  for the outer arms, while for the middle arm it becomes identical to  $v$ . Therefore, for a particular eigenstate  $|\psi_k\rangle$  the persistent current becomes,  $I^k = \langle \psi_k | I | \psi_k \rangle$ , where  $|\psi_k\rangle = \sum_p a_p^k |p\rangle$ . Here  $|p\rangle$ 's are the Wannier states and  $a_p^k$ 's are the corresponding coefficients.

Following the above relations, now we can write down the expressions for persistent currents in the individual branches for a given eigenstate  $|\psi_k\rangle$ . They are as follows.

For the upper arm:

$$I_U^k = \frac{2\pi i e t}{N_U + N_L} \sum_j \left( a_j^{k*} a_{j+1}^k e^{-i\theta_1} - h.c. \right) \quad (3)$$

where, summation over  $j$  spans from 1 to  $N_U$ .

In the case of middle-arm:

$$I_M^k = \frac{\pi i e v}{N_M} \sum_l \left( a_l^{k*} a_{l+1}^k e^{-i\theta_2} - h.c. \right) \quad (4)$$

here, the net contribution comes from  $N_M$  bonds.

Finally, for the case of lower arm:

$$I_L^k = \frac{2\pi i e t}{N_U + N_L} \sum_j \left( a_j^{k*} a_{j+1}^k e^{-i\theta_1} - h.c. \right) \quad (5)$$

In this case the net contribution comes from the lower bonds. The lattice constant  $a$  is set equal to 1.

At absolute zero temperature ( $T = 0$  K), the net persistent current in any branch of the quantum network for a particular electron filling can be obtained by taking sum of the individual contributions from the energy levels with energies less than or equal to Fermi energy  $E_F$ .

Therefore, for  $N_e$  electron system total persistent in any branch becomes  $I_\beta = \sum_k^{N_e} I_\beta^k$ , where  $\beta = U, M$  and  $L$ , for the upper, middle and lower arms, respectively. Once  $I_U, I_M$  and  $I_L$  are known, the net persistent current for the full network can be easily obtained simply adding the contributions of the individual arms, and hence the total current is given by  $I_T = I_U + I_M + I_L$ .

The net persistent current ( $I_T$ ) can also be determined in some other ways as available in the literature. Most probably the easiest way of calculating persistent current is to take first order derivative of ground state energy with respect to magnetic flux<sup>7,8</sup>. However in this method it is not possible to find the distribution of persistent current in individual arms of the network with a high degree of accuracy. On the other hand in our present scheme, the so-called second-quantized approach, there are certain advantages compared to other available procedures. Firstly, we can easily calculate persistent current in any branch of a network. Secondly, the determination of individual responses in separate arms provides much deeper insight to the actual mechanism of electron transport in a transparent way.

In the present work we investigate all the essential feature of magneto-transport at absolute zero temperature and choose the units where  $c = e = h = 1$ . Throughout the numerical work we set  $t = v = -1$  and measure the energy scale in unit of  $t$ .

### III. NUMERICAL RESULTS AND DISCUSSION

#### A. Quantum network with $\epsilon_A = \epsilon_B = 0$

We first start with a perfect quantum system where  $\epsilon_A$  and  $\epsilon_B$  and  $\epsilon_C$  are all identical to each other and we set  $\epsilon_A = \epsilon_B = \epsilon_C = 0$ . To have a clear idea about the magnetic response of the model quantum system, first we illustrate the behavior of energy spectra as a function of flux  $\phi_1$  for different values of flux  $\phi_2$  threaded by the lower sub-ring. The results are presented in Fig. 2, where (a) and (b) correspond to  $\phi_2 = 0$  and  $\phi_0/4$ , respectively. In the absence of flux  $\phi_2$ , energy levels near the edges of the spectrum become more dispersive than those lying in the central region (see Fig. 2(a)) and near the center of the spectrum the energy levels are almost non-dispersive with respect to flux  $\phi_1$ . This feature implies that the persistent current amplitude becomes highly sensitive to the electron filling i.e., the Fermi energy  $E_F$  of the system, since the current is directly proportional to the slope of the energy levels<sup>7</sup>. The situation becomes much more interesting when we add a magnetic flux in the lower sub-ring. Here, the energy levels near the central region of the spectrum becomes more dispersive in nature than the energy levels near the edges (Fig. 2(b)), and it increases gradually with flux  $\phi_2$ , which gives a possibility of getting higher current amplitude with increasing the total number of electrons  $N_e$  in the system. A similar kind of energy spectrum is also observed if we plot the energy

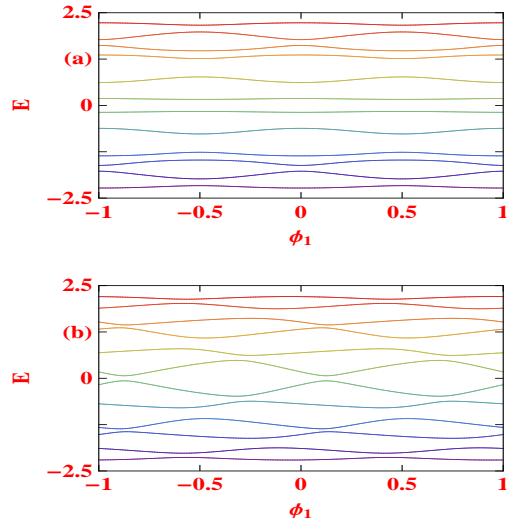


FIG. 2: (Color online). Energy levels as a function of flux  $\phi_1$  for a three-arm ring with  $\epsilon_A = \epsilon_B = 0$  considering  $N_U + N_L = 10$  and  $N_M = 3$ , where (a) and (b) correspond to  $\phi_2 = 0$  and  $\phi_0/4$ , respectively.

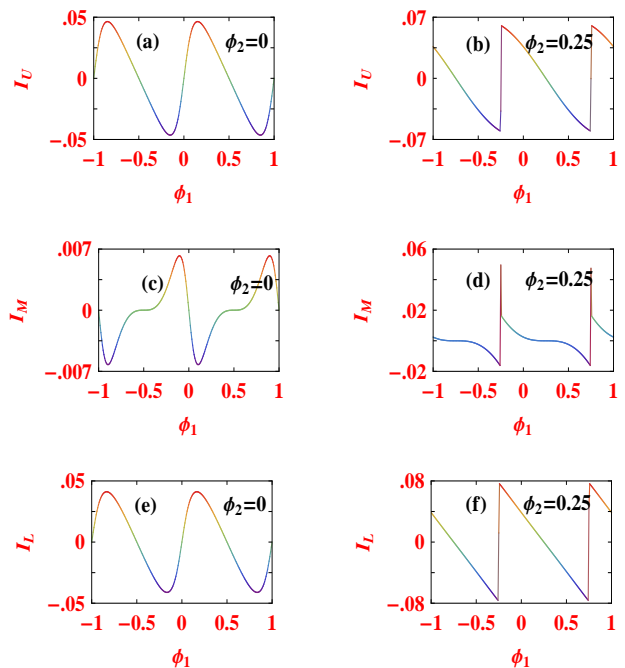


FIG. 3: (Color online). Persistent current in different arms as a function of  $\phi_1$  for a three-arm ring with  $\epsilon_A = \epsilon_B = 0$  in the half-filled band case considering  $N_U + N_L = 60$  and  $N_M = 25$ .

levels as a function of flux  $\phi_2$  instead of  $\phi_1$ , keeping  $\phi_1$  as a constant. All these energy levels exhibit  $\phi_0 (= 1, \text{ in our choice of units } c = e = h = 1)$  flux-quantum periodicity. Thus, for such a simple quantum network persistent current amplitude might be regulated for a particular filling simply by tuning the magnetic flux threaded by anyone of two such sub-rings, and, its detailed descriptions are

available in the sub-subsequent parts.

In Fig. 3 we present the variation of persistent current in individual arms of the three-arm quantum network as a function of flux  $\phi_1$  for some fixed values of  $\phi_2$ . The panels from the top correspond to the results for the upper, middle and lower arms, respectively, and in all these cases

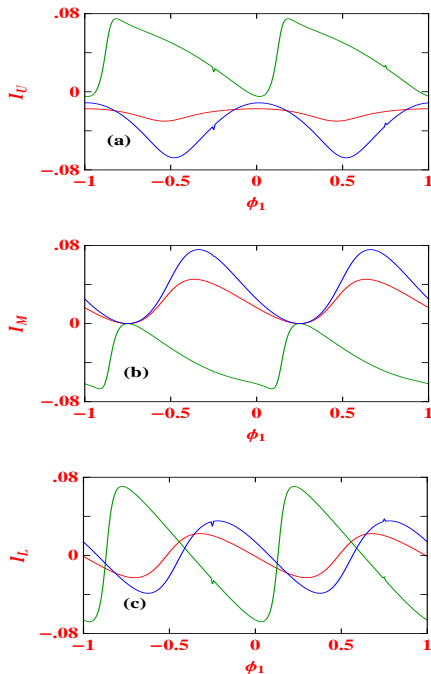


FIG. 4: (Color online). Persistent current in different arms as a function of  $\phi_1$  for a three-arm ring with  $\epsilon_A = \epsilon_B = 0$  considering  $N_U + N_L = 40$  and  $N_M = 17$ . The red, green and blue curves correspond to  $N_e = 10, 15$  and  $20$ , respectively. For all these spectra  $\phi_2$  is set at  $\phi_0/4$ .

the current is determined for the half-filled band case i.e.,  $N_e = 42$ . The left column represents the current for  $\phi_2 = 0$ , and the right column gives the current when  $\phi_2$  is fixed at  $\phi_0/4$ . From the spectra we notice that in some cases current shows continuous like behavior while in some other cases it exhibits saw-tooth like nature as a function of flux  $\phi_1$  threaded by the upper sub-ring. This saw-tooth or continuous like feature solely depends on the behavior of the ground state energy for a particular filling ( $N_e$ ). It is to be noted that in a conventional ordered AB ring we always get saw-tooth like behavior of persistent current irrespective of the filling of the electrons<sup>7</sup>. In the saw-tooth variation a sudden change in direction of persistent current takes place across a particular value of magnetic flux which corresponds to a phase reversal from the diamagnetic nature to the paramagnetic one or vice versa. In our three-arm geometry we also observe that though the current in the upper arm or in the lower arm is not so sensitive to the flux  $\phi_2$ , but the current amplitude in the middle arm changes remarkably, even an order of magnitude, in presence of flux  $\phi_2$ , which leads to a net larger current since the total current is obtained

by adding the contributions from the individual arms.

To explore the filling dependent behavior of persistent current, in Fig. 4 we display persistent currents for three different arms as a function of flux  $\phi_1$  for a typical value of  $\phi_2$ . Here,  $\phi_2$  is set at  $\phi_0/4$ . The red, green and blue lines represent the currents for  $N_e = 10, 15$  and  $20$ , respectively. The current in different arms shows quite a complex structure which strongly depends on the electron filling as well as magnetic flux  $\phi_2$ . In all these cases persistent current provides  $\phi_0$  flux-quantum periodicity, like a traditional single-channel mesoscopic ring or a multi-channel cylinder.

## B. Quantum network with $\epsilon_A \neq \epsilon_B$

Now we focus our attention to the geometry where site energies in the outer arms are no longer identical to each other i.e.,  $\epsilon_A \neq \epsilon_B$ . In this case energy spectrum gets modified significantly compared to the previous one

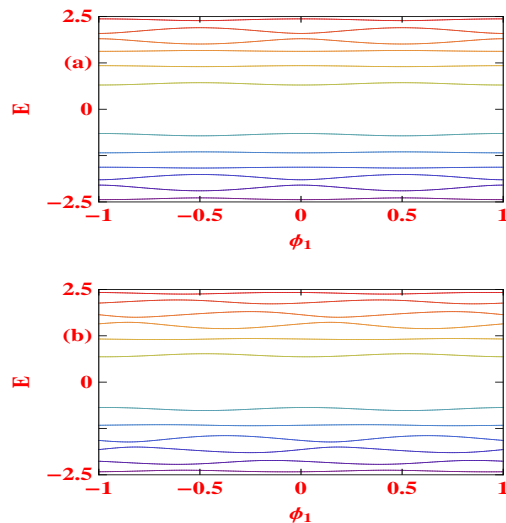


FIG. 5: (Color online). Energy levels as a function of flux  $\phi_1$  for a three-arm ring with  $\epsilon_A = -\epsilon_B = 1$  considering  $N_U + N_L = 10$  and  $N_M = 3$ , where (a) and (b) correspond to  $\phi_2 = 0$  and  $\phi_0/4$ , respectively.

where site energies are uniform ( $\epsilon_A = \epsilon_B$ ). To illustrate it in Fig. 5 we plot the energy-flux characteristics for a three-arm quantum network considering  $\epsilon_A = -\epsilon_B = 1$ , where (a) and (b) correspond to the identical meaning as given in Fig. 2. Since the upper and lower arms of the network are subjected to the binary alloy lattices we get two sets of discrete energy levels spaced by a finite gap around  $E = 0$  (see Fig. 5). Quite interestingly we see that the energy levels near the two extreme edges of the spectrum are more dispersive in nature than those situated along the inner region. With increasing the difference in site energies ( $|\epsilon_A - \epsilon_B|$ ), we get more less dispersive energy levels in the inner region and for large enough value of  $|\epsilon_A - \epsilon_B|$  these levels become almost non-dispersive

and they practically contribute nothing to the current. Thus, for such a system a mixture of quasi-extended and quasi-localized energy levels are found out and it can provide a very large or almost zero current depending on the electron filling. For a very large system size, the energy

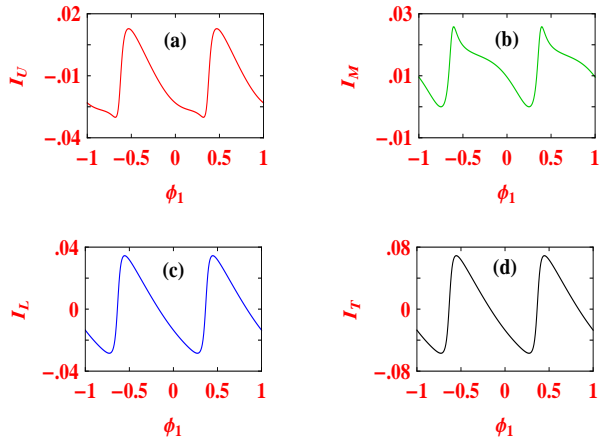


FIG. 6: (Color online). Current-flux characteristics of a three-arm ring with  $\epsilon_A = -\epsilon_B = 1$  considering  $N_U + N_L = 60$ ,  $N_M = 25$  and  $\phi_2 = \phi_0/4$  in the quarter-filled ( $N_e = 21$ ) band case, where (a)-(d) correspond to the currents in the upper, middle and lower arms and in the full system, respectively.

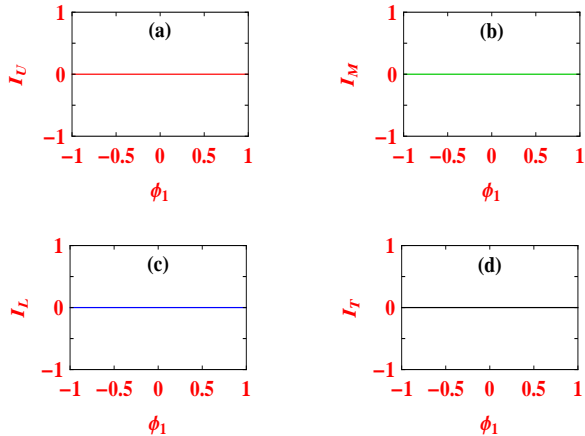


FIG. 7: (Color online). Current-flux characteristics of a three-arm ring with  $\epsilon_A = -\epsilon_B = 1$  in the half-filled ( $N_e = 42$ ) band case for the same parameter values used in Fig. 6.

separation between two successive levels in each set of discrete energy levels gets reduced and we get two quasi-band of energies separated by a finite gap, where the gap is controlled by the parameter values. It is important to note that, unlike the previous one (Fig. 2), for this case the energy spectrum is not so sensitive to flux  $\phi_2$  (Fig. 5). The presence of C-type of atoms in the middle arm which divides the binary alloy ring into two sub-rings is responsible for the existence of quasi-localized energy levels near the inside edges of two quasi-band of energies. Thus we

get more non-dispersive energy levels with increasing the length of the middle arm.

The existence of nearly extended and localized states becomes much more clearly visible from our current-flux spectra. As illustrative example, in Fig. 6 we display the variation of persistent current in individual arms in-

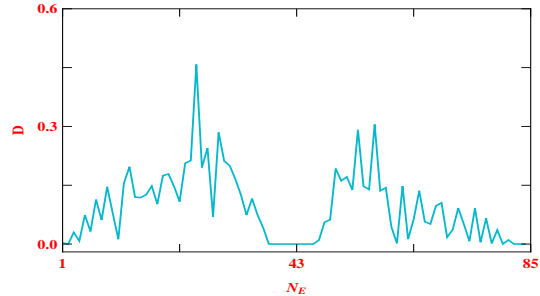


FIG. 8: (Color online). Charge stiffness constant ( $D$ ) as a function of electron filling ( $N_e$ ) for a three-arm ring with  $\epsilon_A = -\epsilon_B = 1$  considering  $N_U + N_L = 60$ ,  $N_M = 25$  and  $\phi_2 = \phi_0/4$ .

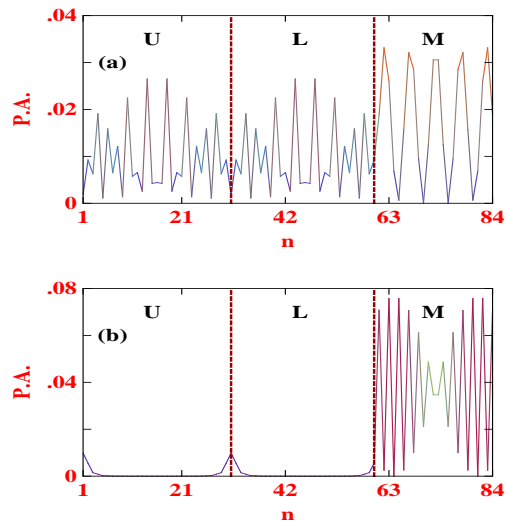


FIG. 9: (Color online). Probability amplitude (P.A.) as a function of site index ( $n$ ) for a three-arm ring with  $\epsilon_A = -\epsilon_B = 1$  considering  $N_U + N_L = 60$  and  $N_M = 25$  when  $\phi_1$  and  $\phi_2$  are set at  $\phi_0/4$ . (a) and (b) correspond to the results of 21-st and 42-nd eigenstates, respectively.

cluding the total current of a three-arm ring considering  $\epsilon_A = -\epsilon_B = 1$  for the quarter-filled ( $N_e = 21$ ) band case. The flux  $\phi_2$  is set equal to  $\phi_0/4$ . From the spectra it is clearly observed that the current in each arm provides a non-zero value (Figs. 6(a)-(c)), and accordingly, the system supports a finite current as shown in Fig. 6(d). The situation becomes completely opposite when the filling factor is changed. Quite remarkably we notice that persistent current almost vanishes in three separate branches which provides almost vanishing net current in the half-filled band case. The results are illustrated in Fig. 7, where (a)-(d) correspond to the identical

meaning as in Fig. 6. The vanishing nature at half-filling and the non-vanishing behavior of current when the system is quarterly filled can be easily understood from the following argument. The total current in any branch or in the complete system mainly depends on the contributions coming from the higher occupied energy levels, while the contributions from the other occupied energy levels cancel with each other. Therefore, for the quarter-filled band case, the net contribution comes from the energy levels which are quasi-extended in nature and a non-zero current appears. On the other hand, for the half-filled band case, the net contribution arises from the levels those are almost localized, and hence, nearly vanishing current is obtained. Thus, we can emphasize that the three-arm ring leads to a possibility of getting high-amplitude to low-amplitude (almost zero) persistent current simply by tuning the filling factor  $N_e$  i.e., the Fermi energy  $E_F$ , and, hence the network can be used as a mesoscopic switch.

The high-conducting to low-conducting switching action with the change of electron filling  $N_e$  in our topology can also be very well explained from the spectrum given in Fig. 8, where we measure the conducting nature by calculating charge stiffness constant, the so-called Drude weight ( $D$ ), in accordance with the idea originally put forward by Kohn<sup>31</sup>. The Drude weight for the system can be easily determined by taking the second order derivative of the ground state energy for a particular filling with respect to flux  $\phi_1$  ( $\phi_1 \rightarrow 0$ ) threaded by the ring<sup>15,31,32</sup>. Kohn has shown that  $D$  decays exponentially to zero for an insulating system, while it becomes finite for a conducting system. A nice feature of the result shown in Fig. 8 is that, the charge stiffness constant almost drops to zero around the half-filled region which reveals the insulating phase, while away from this region it ( $D$ ) has a finite non-zero value that indicates a conducting nature. This feature corroborates the findings presented in Figs. 6 and 7.

To ensure the extended or localized nature of energy eigenstates, finally we demonstrate the variation of probability amplitude (P.A.) of the eigenstates as a function site index  $n$ . The probability amplitude of getting an electron at any site  $n$  for a particular eigenstate  $|\psi_k\rangle$  is obtained from the factor  $|a_n^k|^2$ . Here we analyze the localization behavior for two different energy eigenstates, viz, 21-st and 42-nd states. For the first one the energy

is located well inside a quasi-band, while for the other the energy is placed at the edge of this band. The results are given in Fig. 9 for a three-arm ring with 84 atomic sites. The red dashed lines are used to separate the three distinct regions of the network. In Fig. 9(a) we present the probability amplitudes of the 21st eigenstates and see that the probability amplitude becomes finite for any site  $n$  which indicates that the energy eigenstate is quasi-extended. While, for the other state (42-nd) the probability amplitude almost vanishes at every site of the upper and lower arms of the network. Only at the atomic sites of the middle arm we have finite probability amplitudes. This state does not contribute anything to the current and we can refer the state as a localized one.

#### IV. CONCLUSION

To summarize, in the present work we have explored the magneto-transport properties of a  $\theta$  shaped three-arm quantum ring in the non-interacting electron framework. The upper and lower sub-rings of the network are threaded by magnetic fluxes  $\phi_1$  and  $\phi_2$ , respectively. We have used a single-band tight-binding Hamiltonian to illustrate the model quantum system, where the outer arms are subjected to the binary alloy lattices and the middle arm has identical lattice sites. In the absence of the middle arm, all the energy eigenstates are extended, but the inclusion of the middle arm produces some quasi localized states within the band of extended states and provides a possibility of getting a high conducting state to the low conducting one upon the movement of the Fermi energy. Thus, the system can be used a mesoscopic switch. We have verified the switching action from high-to low-conducting state and vice versa by investigating the persistent current and charge stiffness constant in the network for different band fillings. We have numerically computed both the total current and the individual currents in separate branches by using second-quantized approach. We hope our present analysis may be helpful for studying magneto-transport properties in any complicated quantum network. Finally, we have also examined the nature of the energy eigenstates in terms of the probability amplitude in different sites of the geometry.

---

\* Electronic address: santanu@post.tau.ac.il

<sup>1</sup> A. M. Jayannavar and P. S. Deo, Phys. Rev. B **51**, 10175 (1995).

<sup>2</sup> T. P. Pareek, P. S. Deo, and A. M. Jayannavar, Phys. Rev. B **52**, 14657 (1995).

<sup>3</sup> M. Büttiker, Y. Imry, and R. Landauer, Phys. Lett. **96A**, 365 (1983).

<sup>4</sup> H. F. Cheung, Y. Gefen, E. K. Riedel, and W. H. Shih, Phys. Rev. B **37**, 6050 (1988).

<sup>5</sup> B. L. Altshuler, Y. Gefen, and Y. Imry, Phys. Rev. Lett.

**66**, 88 (1991).

<sup>6</sup> A. Schmid, Phys. Rev. Lett. **66**, 80 (1991).

<sup>7</sup> S. K. Maiti, Physica E **31**, 117 (2006).

<sup>8</sup> S. K. Maiti, Phys. Status Solidi B **248**, 1933 (2011).

<sup>9</sup> S. Belluci and P. Onorato, Physica E **41**, 1393 (2009).

<sup>10</sup> X. Chen, Z. Deng, W. Lu, and S. C. Shen, Phys. Rev. B **61**, 2008 (2000).

<sup>11</sup> H. -C. Wu, Y. Guo, X. -Y. Chen, and B. -L. Gu, Phys. Rev. B **68**, 125330 (2003).

<sup>12</sup> H. -M. Li and J. -L. Xiao, Physica B **396**, 91 (2007).

- <sup>13</sup> H. -M. Li, Y. -L. Huang, and J. -L. Xiao, *Int. J. Mod. Phys. B* **22**, 2255 (2008).
- <sup>14</sup> S. K. Maiti, S. Saha, and S. N. Karmakar, *Eur. Phys. J. B* **79**, 209 (2011).
- <sup>15</sup> S. K. Maiti, M. Dey, S. Sil, A. Chakrabarti, and S. N. Karmakar, *Europhys. Lett.* **95**, 57008 (2011).
- <sup>16</sup> S. K. Maiti, *Solid State Commun.* **150**, 2212 (2010).
- <sup>17</sup> S. K. Maiti, J. Chowdhury, and S. N. Karmakar, *Solid State Commun.* **135**, 278 (2005).
- <sup>18</sup> L. P. Levy, G. Dolan, J. Dunsmuir, and H. Bouchiat, *Phys. Rev. Lett.* **64**, 2074 (1990).
- <sup>19</sup> V. Chandrasekhar, R. A. Webb, M. J. Brady, M. B. Ketchen, W. J. Gallagher, and A. Kleinsasser, *Phys. Rev. Lett.* **67**, 3578 (1991).
- <sup>20</sup> D. Mailly, C. Chapelier, and A. Benoit, *Phys. Rev. Lett.* **70**, 2020 (1993).
- <sup>21</sup> H. Bluhm, N. C. Koshnick, J. A. Bert, M. E. Huber, and K. A. Moler, *Phys. Rev. Lett.* **102**, 136802 (2009).
- <sup>22</sup> P. W. Anderson, *Phys. Rev.* **109**, 1492 (1958).
- <sup>23</sup> D. H. Dunlap, H. L. Wu, and P. W. Phillips, *Phys. Rev. Lett.* **65**, 88 (1990).
- <sup>24</sup> H. -L. Wu and P. Phillips, *Phys. Rev. Lett.* **66**, 1366 (1991).
- <sup>25</sup> Y. M. Liu, R. W. Peng, X. Q. Huang, M. Wang, A. Hu, and S. S. Jiang, *J. Phys. Soc. Jpn.* **72**, 346 (2003).
- <sup>26</sup> X. F. Hu, Z. H. Peng, R. W. Peng, Y. M. Liu, F. Qiu, X. Q. Huang, A. Hu, and S. S. Jiang, *J. Appl. Phys.* **95**, 7545 (2004).
- <sup>27</sup> R. L. Zhang, R. W. Peng, X. F. Hu, L. S. Cao, X. F. Zhang, M. Wang, A. Hu, and S. S. Jiang, *J. Appl. Phys.* **99**, 08F710 (2006).
- <sup>28</sup> A. Chakrabarti, S. N. Karmakar, and R. K. Moitra, *Phys. Rev. B* **50**, 13276 (1994).
- <sup>29</sup> A. Chakrabarti, S. N. Karmakar, and R. K. Moitra, *Phys. Rev. Lett.* **74**, 1403 (1995).
- <sup>30</sup> S. K. Maiti, *J. Appl. Phys.* **110**, 064306 (2011).
- <sup>31</sup> W. Kohn, *Phys. Rev.* **133**, A171 (1964).
- <sup>32</sup> S. K. Maiti, J. Chowdhury, and S. N. Karmakar, *Phys. Lett. A* **332**, 497 (2004).